

Direct Contact Resistance Evaluation of Thermoelectric Legs

Y. Kim^{1,2} · G. Yoon¹ · S. H. Park²

Received: 18 June 2015 / Accepted: 11 January 2016 / Published online: 1 February 2016
© Society for Experimental Mechanics 2016

Abstract In developing intermediate temperature (300–700 °C) thermoelectric modules with high conversion efficiencies exceeding 10 %, the evaluation of the electrical contact resistance between the thermoelectric material and metallic electrode is a critical issue. In this work, a novel direct contact resistance measurement apparatus is proposed that enhances the previously reported extrapolation based erroneous contact resistance evaluation methods. The accuracy and resolution of this apparatus are investigated in detail, and the proposed novel contact resistance measurement exhibits sufficient performance to evaluate high efficiency thermoelectric modules. The presence of the Peltier effect in the direct current-induced contact resistance measurements is verified experimentally using the proposed apparatus. Two modified measurement parameters, i.e., the pulse shape input current and heat dissipating metallic block, are proposed and their effects in suppressing the unintended Peltier effect are discussed in detail.

Keywords Thermoelectric leg · Thermoelectric module · Contact resistance · Peltier effect · Specific contact resistance

✉ S. H. Park
parksh@kier.re.kr

¹ Department of Electrical Engineering, Korea Advanced Institute of Science and Technology (KAIST), 291 Daehak-ro, Yuseong-gu, Daejeon 305-701, Republic of Korea

² Advanced Materials and Devices Laboratory, Korea Institute of Energy Research, 152 Gajung-ro, Yuseong-gu, Daejeon 305-343, Republic of Korea

Introduction

Recent advances in thermoelectric materials operating in intermediate temperature ranges (300–700 °C) have attracted significant attention in the context of developing novel and environmentally-friendly power generation technologies. The well-known thermoelectric material PbTe has been investigated by numerous groups and its highest reported thermoelectric figure of merit (ZT) value is 2.2 at 442 °C [1]. Skutterudite structure series materials have exhibited a ZT value of almost 1.7 at 577 °C [2]. In 2014, Kanatzidis and his group reported a record high bulk-based thermoelectric figure of merit of 2.6 with crystalline SnSe [3]. The development of these novel thermoelectric materials with high ZT performances in the intermediate temperature range demonstrates the practical possibility of power generation efficiency of around 20 % [4, 5].

In order to fabricate thermoelectric modules based on high performance thermoelectric materials, two essential technologies should be developed for practical applications. Due to relatively high temperature operation conditions, these thermoelectric modules are commonly exposed to severe oxidation environments. Accordingly, anti-oxidation technologies should be developed for more appropriate and reliable applications of such intermediate temperature thermoelectric power devices [6–8]. The other important technological issue involves the interfaces between the thermoelectric materials and metallic electrodes. As depicted in Fig. 1(a), a thermoelectric uni-couple consists of both n- and p-type thermoelectric legs and electrodes that electrically connect these two legs in series. The thermoelectric module consists of many uni-couples that are connected in series, as shown in Fig. 1(b). Considering that the same process and material are used to form bonding interfaces on both sides of the thermoelectric leg,

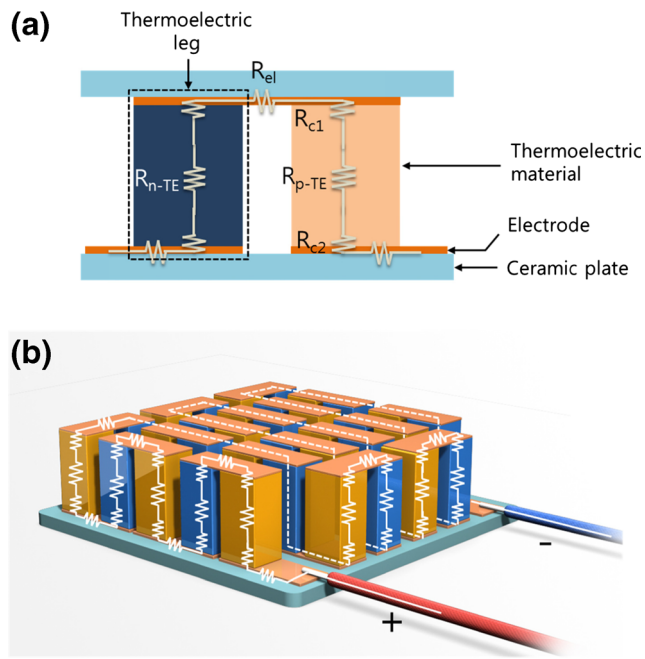


Fig. 1 **a** Structure and resistance components in the thermoelectric leg and **b** the series connection of the resistance components in an intermediate-temperature thermoelectric module

both electrical contact resistances of R_{c1} and R_{c2} in Fig. 1(a) have the same value, i.e., R_c . In this case, for the thermoelectric module with n uni-couples, the total electrical module resistance R_{total} is represented as follows:

$$R_{total} = n(R_{n-TE} + R_{p-TE}) + 2nR_{el} + 4nR_c \quad (1)$$

where R_{n-TE} and R_{p-TE} are the resistances of each type of thermoelectric leg and R_{el} is the resistance of the metallic electrode. When the electrode resistance is significantly smaller than R_{TE} and R_c , equation (1) can be summarized as follows:

$$R_{total} \approx n(R_{n-TE} + R_{p-TE}) + 4nR_c \quad (2)$$

The electrical power that the thermoelectric module can generate at ΔT is summarized as follows:

$$P = \frac{(2S\Delta T)^2}{4R_{total}} = \frac{n(2S\Delta T)^2}{4\{(R_{n-TE} + R_{p-TE}) + 4R_c\}} \quad (3)$$

where S is the Seebeck coefficient of the thermoelectric material. Depending on the different thermoelectric modules, the ratio between R_{TE} and R_c can vary and some previous studies have obtained an R_c ratio in R_{total} of almost 30 % [9]. This indicates that the contact resistance R_c can have a significant impact on the module power output characteristics. In order to develop high output efficient thermoelectric modules, the bonding interfaces must be carefully processed to realize minimum contact resistance [10–12].

In order to develop an appropriate and optimized process for bonding the interface between the thermoelectric material and the electrodes, the contact resistance should be measured precisely to provide a quantitative understanding of various interface bonding results. Several previous studies have addressed this technological issue through proposing various methodologies and apparatus designs [13–19]. One of the most frequently used contact resistance measuring methodologies is the extrapolation technique. This approach was developed several decades ago with limited and insufficient resources of the apparatus and machinery components [19, 20]. This extrapolation method also has inevitable uncertainties in drawing the location of the contact point between the measured resistance extrapolation line and the expected bonding interface location [11, 21].

In this work, a new apparatus design for contact resistance measurements with high accuracy of up to 10^{-6} ohm is proposed, and its performance in evaluating the thermoelectric bonding interface is investigated. An auto-scanning mode probing structure with a micro-motorized moving stage also has been designed and its capability to detect fine and narrow thermoelectric interfaces has been evaluated. The accuracy of the proposed contact resistance measuring apparatus is investigated using pure Cu plate resistivity measurements. Previous contact resistance studies have not addressed the Peltier effect that arises during the DC current input measurement of thermoelectric materials. This work clearly identifies the presence of an erroneous Peltier effect under the DC current contact resistance measurements. Moreover, to eliminate the undesirable Peltier effect in the contact resistance measurements, two measurement techniques (a pulse-shaped AC input current mode and a heat dissipating contact block) are proposed and the related electrical contact resistance measurement results are discussed in detail.

Theory and Experiments

Thermoelectric bulk resistance (R_{TE} in Fig. 1(a)) is mainly determined when the thermoelectric materials are processed. The inherent resistance of the thermoelectric leg cannot be modified solely for the purpose of minimizing the total resistance of the thermoelectric module because this type of material modification will also affect, and usually deteriorate, other important thermoelectric characteristics such as the Seebeck coefficient and thermal conductivity. Considering these typical resistance characteristics of thermoelectric materials, the interfacial contact resistance is the most important parameter in terms of practically improving the efficiency of thermoelectric modules.

The definition of electrical contact resistance is the interfacial resistance that is established at the interface of two materials. In order to distinguish this from the bulk

resistance, the specific contact resistance is defined as follows:

$$\rho_c = R_c \times A \ (\Omega \cdot \text{cm}^2), \quad (4)$$

where R_c is the electrical contact resistance and A is the apparent contact area of the interface. Because this interface is located inside the jointed bulk sample, it is not easy to precisely evaluate the specific contact resistance using the usual bulk resistance measurement method. In order to measure this specific contact resistance correctly from the bulk resistances on both sides of the interface, an exclusive measurement apparatus is necessary.

Various types of thermoelectric materials were fabricated to evaluate the proposed contact resistance measurement apparatus. A chalcogenide thermoelectric material of SnSe was synthesized and ingots were processed via spark plasma sintering (SPS). Two Cu electrode plates with thickness of 800 μm were bonded on both sides of the SnSe pellets using diffusion bonding technology via low-vacuum hot pressing at around 500 $^\circ\text{C}$. The electrode bonded pellets were mechanically sliced and surface-polished for the contact resistance measurements. Commercially available calcium manganese oxide thermoelectric legs and Bi_2Te_3 legs were also prepared to measure the interfacial contact resistance. As shown in Fig. 2, the novel contact resistance measurement apparatus was designed and fabricated. This apparatus was designed to

directly measure the electrical contact resistance of the thermoelectric leg interface without extrapolation. This probing system primarily consists of a motorized stage, a micro-positioner, source current input blocks with a spring tension structure, and a USB digital microscope. The probing configuration utilizes the four-wire probe method to minimize unnecessary contact resistance effects between the voltage probe tip and sample surface. The motorized stage that moves along the horizontal axis has a 2 μm resolution moving step. The micro-positioner was equipped with a commercial spring probe pin (P15-51, Modusystems, Inc.) with a skewed angle installation. During the scanning measurement steps, the inclined spring probe was fixed in its original position and the motorized stage was moved along the entire measurement length. For input source current contact to measure the thermoelectric sample, Cu blocks with several dimensions were prepared (1.15 cm^2 , 2.25 cm^2 , and 4.5 cm^2). The spring compressions on both sides of the thermoelectric leg were controlled using a manual screw with a spring constant of $k=7.84 \text{ N/cm}$, which enabled application of the maximum pressure of about 500 kPa on each side of the tested sample. A digital current source (Keithley 6221 AC and DC current source), which could apply various types of currents, was used for the four-wire principle voltage measurements, as depicted in Fig. 2(a). This current source can generate both DC and pulse-shaped input currents up to 100 mA with 0.15 % uncertainty. To prevent possible electromagnetic perturbations, all electrical lines were designed with coaxial wires. Moreover, for electrical white noise shielding, the measuring apparatus was covered with a full metallic case.

Results and Discussion

Direct Electrical Contact Resistance Measurement Using a Scanning Probe

Electrical contact resistance measurements in previous studies generally use a hard metal probe (e.g., tungsten) that makes contact with the measured thermoelectric leg surface. This sharp, hard probe tip can produce scratches on the thermoelectric sample surface and cause movement errors in repeated probing steps. To prevent these drawbacks of a hard probe, this work utilized a spring probe to scan the resistance value while the contacted thermoelectric leg was moving, as shown in Fig. 3(a). The resistance measurement results in Fig. 3(b) clearly indicate that the proposed scanning spring probe is suitable for direct contact resistance evaluation. Figure 3 presents the results of the evaluation of a diffusion-bonded Cu/SnSe/Cu structure thermoelectric leg sample. The obtained scanning line indicates that there was a 379 $\mu\Omega$ resistance difference at the interface between Cu and SnSe, which represents the electrical contact resistance of the tested

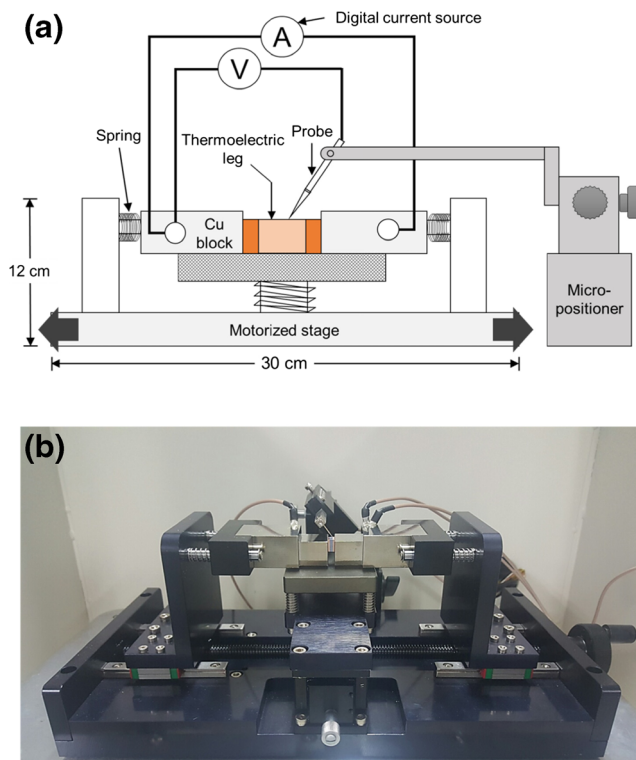


Fig. 2 a Schematic and b photograph of the proposed electrical contact resistance measurement apparatus for a thermoelectric leg

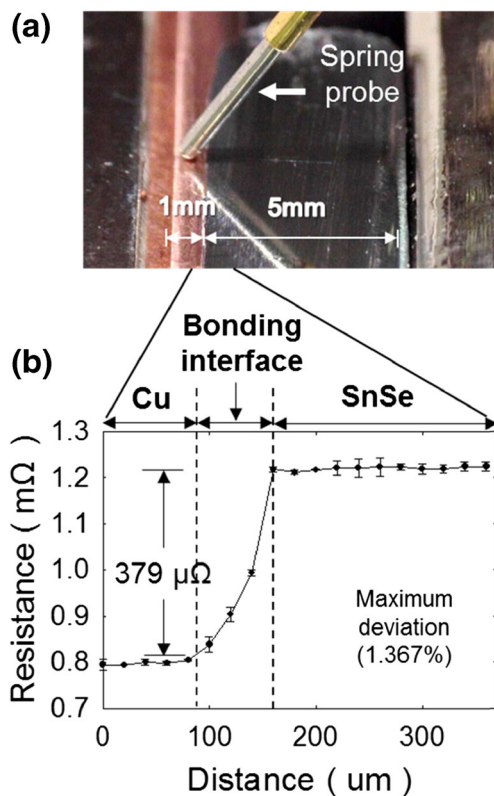


Fig. 3 **a** Photograph of the contacted spring probe on the diffusion-bonded Cu/SnSe/Cu thermoelectric leg surface and **b** the averaged resistance results from five repeated measurements and their deviations

Cu/SnSe/Cu thermoelectric leg. Five repeated measurements exhibited consistent resistance traces with a maximum of 1.367 % deviation. The resistance line trace in Fig. 3 demonstrates that this SnSe thermoelectric leg has a bonding interface thickness of around 60 μm. The scanned resistance results in Fig. 3 clearly show that the proposed probing method can directly measure the thermoelectric interface resistance difference (electrical contact resistance) and the thickness of the resistance transition layer without extrapolation.

Pressure Effects in Electrical Contact Resistance Measurement

As shown in Fig. 2, the thermoelectric leg sample is located on the motorized stage and fixed by the Cu blocks on both sides of the sample electrodes. To establish tight contact between these Cu blocks and the thermoelectric leg, each Cu block is forced by the spring structure, which has a spring constant of 7.78 N/cm, as indicated in Fig. 4(a). The effect of this compressive sample holding pressure on the contact resistance measurement has been investigated using the diffusion-bonded Cu/SnSe/Cu sample and the results are presented in Fig. 4(b). At two relatively low compressive pressures of 50 kPa and 100 kPa, the resultant resistance varies from 5.8 to 3.7 mΩ on the Cu electrode side. This resistance variation

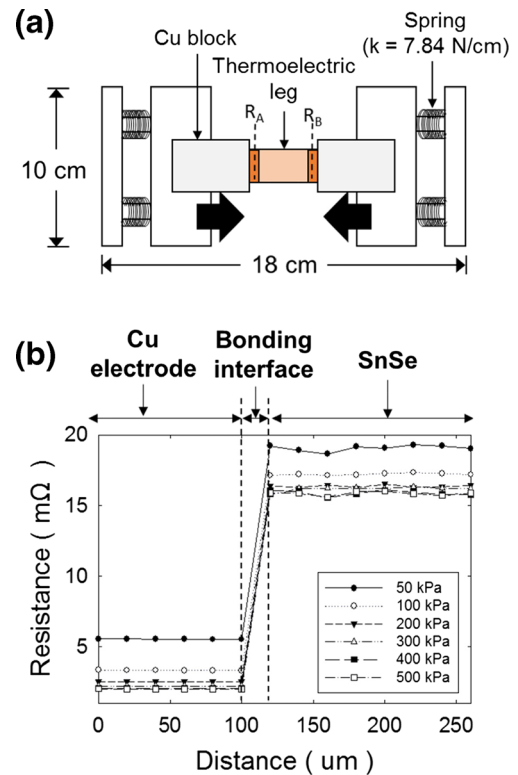


Fig. 4 **a** Schematic of the thermoelectric leg holding pressure stage and **b** the resistance measurement results according to various compressive pressure conditions

disappears with compressive pressures from 200 to 500 kPa. The higher resistances at pressures of 50 kPa and 100 kPa primarily resulted from insufficient contact between the Cu electrode and the Cu block. Although both surfaces were flatly polished for appropriate contact, some irregularities in the flat polished plane created an unexpected gap between these two surfaces. At a relatively low compression, this gap remained between the Cu block and the thermoelectric sample, and it caused high contact resistance. At higher compressive pressures, this gap was minimized or removed, and the resultant contact resistance between the Cu block and thermoelectric sample remained the same. Figure 4(b) demonstrates that in the thermoelectric leg contact resistance measurement, and proper compressive pressure (in this case, higher than 200 kPa) should be loaded on both sides of the sample to properly measure the electrical contact resistance.

Accuracy and Resolution of the Electrical Contact Resistance Measurement

In order to verify the resistance measurement accuracy of the proposed apparatus, a pure Cu plate of 99.99 % was prepared with fine surface polishing. The accuracy of the apparatus was evaluated through a comparison between the previously reported Cu element resistivity and the measurement results in

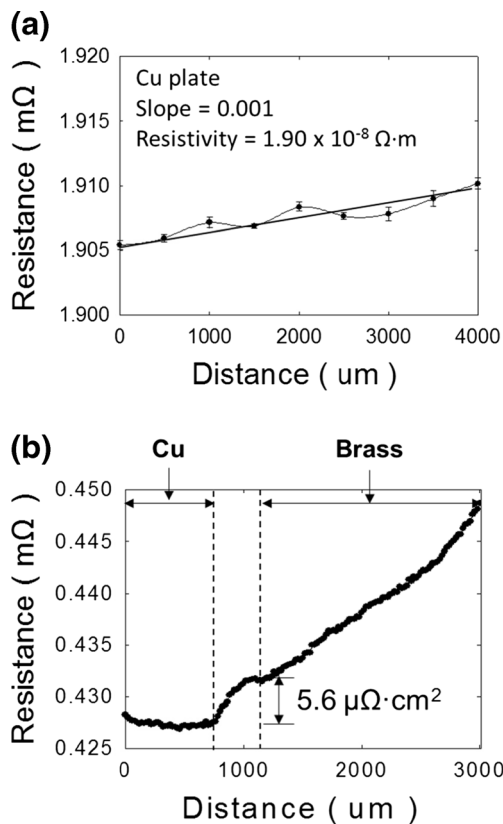


Fig. 5 **a** Cu resistivity measurement results from the resistance scanning graph and **b** specific contact resistance results of the Cu-Brass functionally graded material (FGM) interface

this work. The resistivity of the pure Cu plate was measured using the resistance graph in Fig. 5(a). The resistivity of the sample is defined as follows:

$$\rho = \frac{R}{L} \times A \text{ (}\Omega\cdot\text{cm)} \quad (5)$$

where L is the measurement distance and A is the cross-sectional area of the tested sample. The slope of the resistance graph (R/L) in Fig. 5(a) is equal to ρ/A from equation (5), and the area of the Cu plate was $1.9 \times 10^{-5} \text{ m}^2$. From this equation relation, the Cu plate resistivity was obtained as $1.90 \times 10^{-8} \Omega \cdot \text{m}$. The measured Cu resistivity is very close to the Cu resistivity of $1.68 \times 10^{-8} \Omega \cdot \text{m}$ at 20°C found in the literature [22], and this comparison clearly indicates that the proposed apparatus has high accuracy in measuring resistance values.

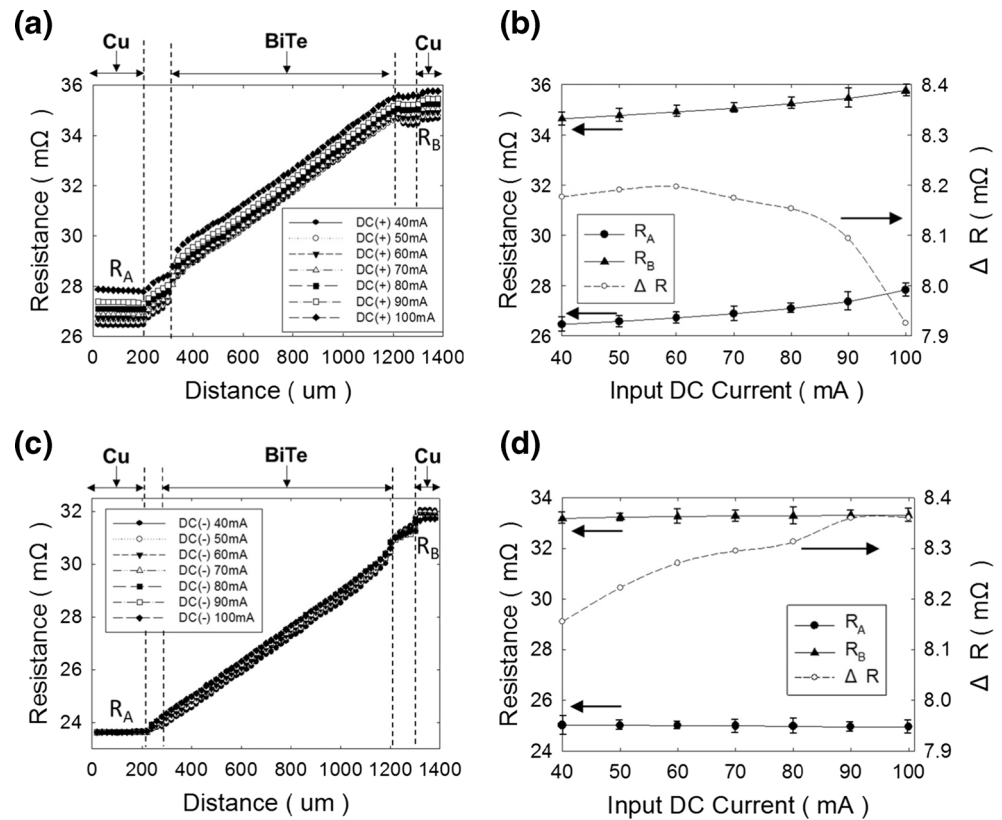
The resolution of the proposed contact resistance apparatus was evaluated experimentally. A functionally graded material (FGM) Cu and brass joint sample was fabricated using SPS. The resultant specific contact resistance of the interface of the two different metals was $5.6 \mu\Omega \cdot \text{cm}^2$, as shown in Fig. 5(b). The resistance scanned results in Fig. 5(b) demonstrate that the proposed measurement apparatus can distinctly capture small resistance variations at a scale of $10^{-6} \Omega \cdot \text{cm}^2$. Recent

research results of intermediate temperature thermoelectric modules from General Motors (GM) and MIT reported that their best performance modules had specific contact resistances of $30 \times 10^{-6} \Omega \cdot \text{cm}^2$ and $2 \times 10^{-6} \Omega \cdot \text{cm}^2$, respectively [23, 24]. Considering that these two research groups' module performances were the highest reported to date globally, the specific contact resistance value required for a high performance thermoelectric module is several $10^{-6} \Omega \cdot \text{cm}^2$. The results in Fig. 5(b) demonstrate that the measurement using the proposed apparatus meets the required specific contact resistance measuring resolution.

Peltier Effects on the DC Input Current Measurement

Most previous studies that evaluate the electrical contact resistance have utilized a DC current as the source input current [13, 14]. However, the DC current flowing into the thermoelectric leg inevitably induces a Peltier effect, which results in a thermal temperature gradient across the tested sample. This unintended temperature gradient on the thermoelectric leg can affect the resistance evaluation results and provide different resistance curves compared with the constant temperature maintained resistance measurements. In Fig. 6(a) and (c), the measured resistance curves of the same Cu/Bi₂Te₃/Cu thermoelectric leg with opposite DC input current directions are compared. Both measurements exhibited resistance curve variations depending on the injected DC current levels and identified contact interfaces. In order to verify the Peltier effects in the DC current measurement, the resistance differences of both Cu electrodes (R_A and R_B in Fig. 4) are investigated in Fig. 6(b) and (d). For the positive DC direction measurement (Fig. 6(b)), both R_A and R_B show slight increments with increases in the DC level from 40 to 100 mA. However, the differences of these two resistances in the ΔR curve demonstrate that the differences decrease with an increase in the DC level. In the negative DC direction measurement in Fig. 6(d), the resistance differences ΔR increase as the input DC level increases. If the input DC level only induced Joule heating through the thermoelectric leg length, the differences between two electrodes R_A and R_B should be the same regardless of the input DC level variation. However, the opposite variations of resistance differences ΔR in Fig. 6(b) and (d) indicate that there is an additional effect on the resistance measurement that increases or decreases according to the DC current direction alone. This unintended effect is a Peltier effect, which causes both local heating on one side of the sample and cooling on the other side depending on the DC current direction. Figure 6 verifies that the DC input current in the electrical contact resistance evaluation inevitably induces the Peltier effect during the resistance measurement, and this unintended effect may deteriorate the accuracy of the electrical contact resistance measurement due to the local heating and cooling.

Fig. 6 Resistance scanning results of the Cu/Bi₂Te₃/Cu thermoelectric leg with (a) a positive DC input current, and (b) the resistance differences of both electrodes. Resistance scanning results with (c) negative DC input current, and (d) the resistance differences of both electrodes



Peltier Effects on the Pulse Shape Input Current Measurement

In order to prevent the Peltier effect in the DC current measurement, the pulse shape current is utilized, as explained in Fig. 7(a). This rectangular-shaped pulse current alternates positive and negative levels with the designated pulse width. The practical measurement is placed at the end of each pulse width is marked as M_1 , M_2 , and M_3 in Fig. 7(a). The measured results average these separate measuring points using the following: $(M_1 + M_3 - 2M_2)/4$. The resultant resistance curves are presented in Fig. 7(b) according to the pulse heights. The pulse input current measurement in Fig. 7(b) exhibits a similar resistance curve shape to the DC current measurement in Fig. 6, and it clearly identifies the contact interface location of the Cu/Bi₂Te₃/Cu thermoelectric leg. The resistance differences of each Cu electrode (R_A and R_B in Fig. 4) are also evaluated in Fig. 7(c). Unlike the resistance difference variations in Fig. 6(b) and (d), the pulse input measurements exhibited almost identical resistance differences ΔR in all different pulse input levels. This consistency in ΔR means that a significant resistance difference was not measured for both sides of the thermoelectric leg during the pulse input contact resistance measurement. This reinforces that the Peltier effect was absent with the pulse input current measurement, which induces different local temperature gradients at the sides of the

thermoelectric leg and a resultant resistance difference ΔR variation, as seen in Fig. 6(b) and (d).

The elimination of the Peltier effect in the pulse input current measurement is evaluated in the specific contact resistance results in Fig. 8. The interfacial contact resistance from the DC input current measurement shows different and decreasing resistance results with increases in the input current levels for both directions of the DC current. Figure 8 reveals that the contact resistance measurement with the DC input current provides different measurement results depending on the input signal levels and that it has a clear limitation in evaluating electrical contact resistance characteristics. However, the pulse-shaped input current measurement provides consistent specific contact resistance results of approximately $7 \mu\Omega \cdot \text{cm}^2$ regardless of the input current level. This work clearly verifies that the specific contact resistance should be measured with a pulse-shaped input current because the DC current measurement provides erroneous contact resistance results.

Heat Dissipation Effects by Contact Metal Blocks

For a more detailed understanding of the Peltier effect on the DC current measurements, thermal images of the tested oxide thermoelectric leg were examined, as shown in Fig. 9. The local temperature gradient resulting from the Peltier effect is

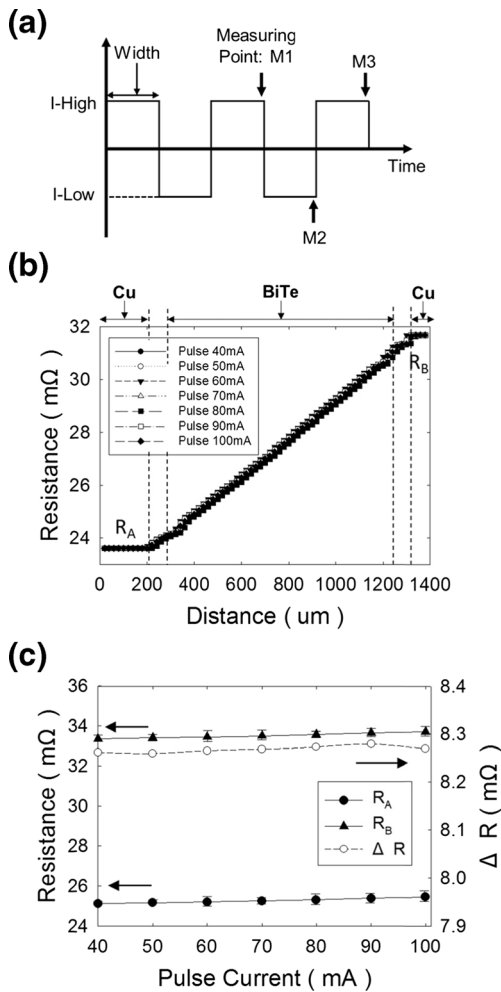


Fig. 7 a Waveform of the pulse shape current source, b resistance scanning results of the Cu/Bi₂Te₃/Cu thermoelectric leg with a pulse input current, and c the resistance differences of both electrodes

clearly detected in Fig. 9(e) at a DC current level of 500 mA. The thermal image indicates that a temperature variation of 2.3 °C occurred in the leg. In Fig. 9(b), (d), and (f), the same oxide thermoelectric leg was placed between the Cu blocks, whereas in Fig. 9(c) and (e), this thermoelectric leg was

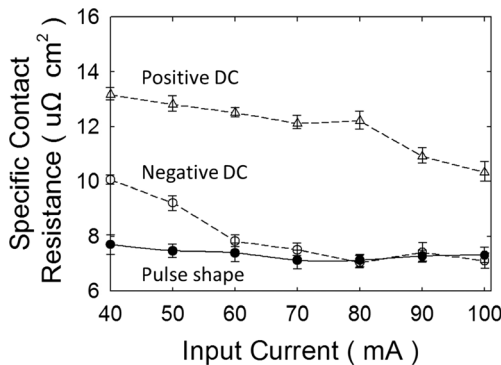


Fig. 8 Comparison of the specific contact resistance measurement results depending on the input current

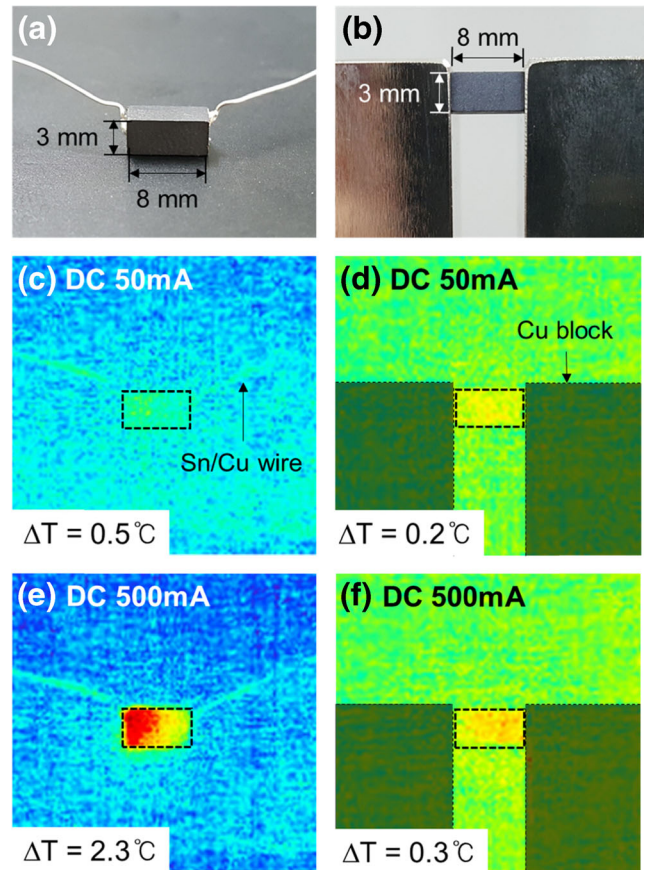


Fig. 9 Photographs of the (a) oxide thermoelectric leg connected to the Sn/Cu wire and (b) oxide leg loaded on the Cu blocks. Thermal images of the oxide leg under a DC bias of 50 mA with (c) Sn/Cu wire and (d) Cu blocks. Thermal images of the oxide leg under a DC bias of 500 mA with (e) Sn/Cu wire and (f) Cu blocks

simply connected to the Sn/Cu wire to investigate the temperature gradient effect without heat dissipation. At a DC level of 50 mA in Fig. 9(c) and (d), both images exhibited similar results without significant temperature gradient. Unlike this low DC level case, the thermal images at 500 mA show significantly different results. The temperature gradient in Fig. 9(e) disappeared in Fig. 9(f), despite the applied DC input current being identical at 500 mA. This primarily resulted from the Cu blocks in Fig. 9(f) fully dissipating and neutralizing the local temperature gradient of the oxide thermoelectric leg that was induced by the Peltier effect. Because the proposed Cu blocks had sufficient size and contact area, additional thermal distribution by the Peltier effect was not found in Fig. 9(f).

Conclusion

A novel contact resistance measurement apparatus was proposed and its characteristics in evaluating various thermoelectric legs were investigated in detail. The proposed scanning

probe method showed direct contact resistance measurement capability with a resolution of up to several $10^{-6} \Omega \cdot \text{cm}^2$ without requiring inaccurate extrapolation processes. Furthermore, the proposed direct measurement technique provided additional information of the contact bonding width. The accuracy performance of the proposed apparatus was verified using pure Cu plate resistivity measurements.

The contact resistance measurements with a DC input current source were investigated, and the presence of the Peltier effect during the measurements was discussed. The comparison of the resistance differences on the electrode sides verified that an unintended Peltier effect appeared and affected the contact resistance results regardless of the DC input current direction. This implies that most previous electrical contact resistance measurements of thermoelectric legs utilizing DC current inputs have not considered this inevitable error in their analyses. In order to prevent this effect in the thermoelectric leg, pulse-shaped alternating input currents were defined and the effect was that the electrical contact resistance did not exhibit Peltier effects in the resistance measurements. The comparison of the resultant specific contact resistances with DC and pulse-shaped current showed that only the pulse-shaped alternating current measurement could provide single consistent contact resistance results regardless of the input current level. Moreover, metallic contact blocks, which have heat dissipating characteristics, could also assist in neutralizing the local temperature gradients that result from the Peltier effect.

The apparatus proposed in this work exhibited accurate contact resistance measurements with a sufficiently fine resolution and elimination of the Peltier effect. Accurate thermoelectric analyses are essential in developing intermediate temperature thermoelectric modules with high conversion efficiencies exceeding 10 %.

Acknowledgments This work was conducted under the framework of the Research and Development Program of the Korea Institute of Energy Research (KIER, B6-2448). This research was also supported by the K-Valley Research, Education, Development & Business Project (RED&B, N01150329) funded by the Korea Advanced Institute of Science and Technology (KAIST). This research was also supported by the National Research Foundation of Korea (NRF) Grant funded by the Korean Government (MSIP) (NRF-2015R1A5A1036133).

References

- Biswas K, He J, Blum ID, Wu CI, Hogan TP, Seidman DN, Dravid VP, Kanatzidis MG (2012) High-performance bulk thermoelectrics with all-scale hierarchical architectures. *Nature* 489:414–418. doi:10.1038/nature11439
- Shi X, Yang J, Salvador JR, Chi M, Cho JY, Wang H, Bai S, Yang J, Zhang W, Chen L (2011) Multiple-filled skutterudites: high thermoelectric figure of merit through separately optimizing electrical and thermal transports. *J Am Chem Soc* 133:7837–7846. doi:10.1021/ja111199y
- Zhao LD, Lo SH, Zhang Y, Sun H, Tan G, Uher C, Wolverton DVP, Kanatzidis MG (2014) Ultralow thermal conductivity and high thermoelectric figure of merit in SnSe crystals. *Nature* 508:373–377. doi:10.1038/nature13184
- Hendricks T, Choate, WT (2006) Engineering scoping study of thermoelectric generator systems for industrial waste heat recovery. Industrial Technologies Program, U.S. DOE. https://www1.eere.energy.gov/manufacturing/industries_technologies/imf/pdfs/teg_final_report_13.pdf
- Shakouri A (2011) Recent developments in semiconductor thermoelectric physics and materials. *Annu Rev Mater Res* 41:399–431. doi:10.1146/annurev-matsci-062910-100445
- Park YS, Thompson T, Kim YS, Salvador JR, Sakamoto JS (2015) Protective enamel coating for n- and p-type skutterudite thermoelectric materials. *J Mater Sci* 50:1500–1512. doi:10.1007/s10853-014-8711-4
- Battiston S, Boldrini S, Fiameni S, Famengo A, Fabrizio M, Barison S (2012) Multilayered thin films for oxidation protection of Mg₂Si thermoelectric material at middle–high temperatures. *Thin Solid Films* 526:150–154. doi:10.1016/j.tsf.2012.10.114
- Zawadzka K, Godlewska E, Mars K, Nocun M (2012) Oxidation resistant coatings for CoSb₃. 9th European conference on thermoelectrics: ECT2011, 1449:231–234. doi:10.1063/1.4731539
- Ebling D, Bartholomé K, Bartel M, Jäggle M (2010) Module geometry and contact resistance of thermoelectric generators analyzed by multiphysics simulation. *J Electron Mater* 39:1376–1380. doi:10.1007/s11664-010-1331-0
- Caillat T, Fleurial JP, Snyder GJ, Zoltan A, Zoltan D, Borshchevsky A (1999) Development of a high efficiency thermoelectric unicouple for power generation applications. 18th international conference on thermoelectrics, pp. 473–476
- Liao CN, Lee CH, Chen WJ (2007) Effect of interfacial compound formation on contact resistivity of soldered junctions between bismuth telluride-based thermoelements and copper. *Electrochem Solid-State Lett* 10:23–25. doi:10.1149/1.2749330
- Tanji Y, Nakagawa Y, Kisara K, Yasuoka M, Moriya S, Kumagai T, Niino M, Sato R (1999) Electric and thermal contact resistances of the new type thermoelectric module assembled by screwing method. 18th international conference on thermoelectrics, pp. 260–265
- Thimont Y, Lognoné Q, Goupil C, Gascoin F, Guilmeau E (2014) Design of apparatus for Ni/Mg₂Si and Ni/MnSi_{1.75} contact resistance determination for thermoelectric legs. *J Electron Mater* 43:2023–2028. doi:10.1007/s11664-013-2940-1
- Liu W, Wang H, Wang L, Wang X, Joshi G, Chen G, Ren Z (2013) Understanding of the contact of nanostructured thermoelectric n-type Bi₂Te_{2.7}Se_{0.3} legs for power generation applications. *J Mater Chem A* 1:13093–13100. doi:10.1039/C3TA13456C
- Gupta RP, McCarty R, Sharp J (2014) Practical contact resistance measurement method for bulk Bi₂Te₃-based thermoelectric devices. *J Electron Mater* 43:1608–1612. doi:10.1007/s11664-013-2806-6
- Buist RJ, Roman SJ (1999) Development of a burst voltage measurement system for high-resolution contact resistance tests of thermoelectric heterojunctions. 18th international conference on thermoelectrics, pp 249–251
- Hogan TP, Downey A, Short J, D'Angelo J, Wu C, Quarez E, Androulakis J, Poudeu PF, Sootsman JR, Chung D, Kanatzidis MG, Mahanti SD, Timm EJ, Schock H, Ren F, Johnson J, Case ED (2007) Nanostructured thermoelectric materials and high-efficiency power-generation modules. *J Electron Mater* 36:704–710. doi:10.1007/s11664-007-0174-9
- de Boor J, Gloanec C, Kolb H, Sottong R, Ziolkowski P, Müller E (2015) Fabrication and characterization of nickel contacts for magnesium silicide based thermoelectric generators. *J Alloys Compd* 632:348–353. doi:10.1016/j.jallcom.2015.01.149
- Berger HH (1972) Contact resistance and contact resistivity. *J Electrochem Soc* 119:507–514



20. Mengali OJ, Seiler MR (1962) Contact resistance studies on thermoelectric materials. *Adv Energy Convers* 2:59–68. doi:[10.1016/0365-1789\(62\)90008-5](https://doi.org/10.1016/0365-1789(62)90008-5)
21. Zhao D, Geng H, Chen L (2012) Microstructure contact studies for skutterudite thermoelectric devices. *Int J Appl Ceram Technol* 9: 733–741. doi:[10.1111/j.1744-7402.2011.02703.x](https://doi.org/10.1111/j.1744-7402.2011.02703.x)
22. Gancoli D (2009) *Physics for scientists & engineers with modern physics*, 4th edn. Prentice Hall, [Upper Saddle River](https://www.wiley.com), p 658. ISBN 0-13-149508-9
23. Salvador JR, Cho JY, Ye Z, Moczygemba JE, Thompson AJ, Sharp JW, König JD, Maloney R, Thompson T, Sakamoto J, Wang H, Wereszczak AA, Meisner GP (2013) Thermal to electrical energy conversion of skutterudite-based thermoelectric modules. *J Electron Mater* 42:1389–1399. doi:[10.1007/s11664-012-2261-9](https://doi.org/10.1007/s11664-012-2261-9)
24. Muto A (2011) *Thermoelectric device characterization and solar thermoelectric system modeling*. Dissertation, University of Massachusetts Institute of Technology